Tunable microlens arrays actuated by various thermo-responsive hydrogel structures



2010 J. Micromech. Microeng. 20 115035

(http://iopscience.iop.org/0960-1317/20/11/115035)

J. Micromech. Microeng. **20** (2010) 115035 (11pp) doi:10.1088/0960-1317/20/11/115035

# Tunable microlens arrays actuated by various thermo-responsive hydrogel structures

**Xuefeng Zeng**[1,4], **Chenhui Li**[1,4], **Difeng Zhu**[1], **Hyung Joon Cho**[1] **and Hongrui Jiang**[1,2,3]

[1] Electrical and Computer Engineering, University of Wisconsin–Madison, Madison, WI, USA
[2] Eye Research Institute, University of Wisconsin–Madison, Madison, WI, USA
[3] Materials Science Program, University of Wisconsin–Madison, Madison, WI, USA

Received 15 July 2010, in final form 12 September 2010
Published 25 October 2010
Online at stacks.iop.org/JMM/20/115035

**Abstract**
We report on liquid-based tunable-focus microlens arrays made of a flexible polydimethylsiloxane (PDMS) polymer. Each microlens in the array is formed through an immiscible liquid–liquid interfacial meniscus. Here deionized water and silicone oil were used. The liquids were constrained in the PDMS structures fabricated through liquid-phase photopolymerization for molding and soft lithography. The microlenses were actuated by thermo-responsive *N*-isopropylacrylamide (NIPAAm) hydrogel microstructures and could be tuned individually by changing the local temperature. The NIPAAm hydrogels expanded and contracted, absorbing and releasing water, at different temperatures. Thus the pressure across the water–oil interface in the microlenses varied responding to the temperature, tuning their corresponding focal lengths. The microlens diameter was 2.4 mm. The typical microlens focal length was measured to be from 8 to 60 mm depending on the temperature. The microlens response time actuated by different structures and components of the NIPAAm hydrogels were compared. The normalized light intensities of the microlens focused spots were measured, matching well with a Zemax simulation, to study the microlens spherical aberrations. The NIPAAm hydrogel durability was also measured.

(Some figures in this article are in colour only in the electronic version)

## 1. Introduction

Emerging liquid-based tunable-focus optical microlenses play an important role in both modern photonics and micro-optics [1]. They are extensively used in a wide range of applications such as optoelectronics and photonic devices, as well as in image processing [2–11]. These microlenses are formed through an air–liquid or liquid–liquid interface or covered by a flexible membrane. The interface or membrane deforms when a pressure is applied, adjusting the radius of curvature of the spherical interface or membrane and consequently the focal length of the microlenses. The pressure on the interface or membrane could be dynamically applied by mechanical pressure [2, 3] or displacement [4], electromagnetic field [5], electrochemistry [6], electrowetting [7–9] or dielectrophoretic effect [10, 11]. These microlenses require external controls and power supplies; for example, high voltage or large current are necessary for electrically controlled microlenses and an external actuation device is required to control the pneumatic pressure or displacement of the flexible membrane. The additional components increase the size and limit the integration of the whole system, challenging their applications, especially in lab-on-a-chip and biomedical devices.

We recently reported a single liquid-based, tunable-focus microlens actuated by stimuli-responsive hydrogels which could respond to temperature [12, 13], pH [14] and infrared light [15]. Stimuli-responsive hydrogels are materials that undergo a significant and reversible volumetric change in response to environmental stimuli by absorbing water into or releasing water from the network of the hydrogels [16]. Here, we present such a microlens array in which

[4] These authors contributed equally to this work.

 

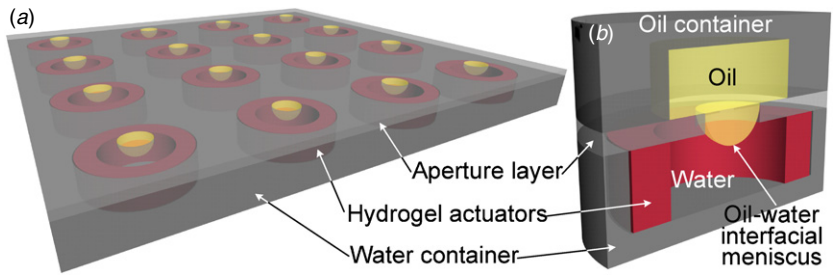


**Figure 1.** (*a*) Schematic of a liquid-based tunable-focus microlens array consisting of 4 × 4 microlenses. (*b*) 3D cross-sectional view of one microlens in the microlens array. The microlens is formed through an immiscible liquid–liquid interface. Here deionized water and silicone oil are used. A polymer plate with an aperture hole, called the aperture layer, separates oil and water, forming a water container and an oil container. For better visibility, the oil container is not illustrated in (*a*). The sidewall of the aperture and the bottom surface of the plate are chemically treated hydrophilic, while the top surface of the plate is naturally hydrophobic, generating a hydrophilic–hydrophobic (H–H) boundary at the top edge of the aperture. The water–oil interfacial meniscus is pinned by this H–H boundary and serves as a microlens. The hydrogels in the water container, as the actuators, shrink and release water at high temperature; and expand and absorb water at room temperature. The pressure in the water container changes responding to the change in the local temperature, moving the water–oil meniscus and varying the microlens focal length.

each microlens is individually actuated by thermo-responsive hydrogel microstructures. The microlens array was planar and was made of flexible polymers, suitable for potential curvilinear substrates [17]. Images from the microlenses were recorded and their focal length was measured. The effect of various structures and components of the hydrogels on the microlens response time were compared. The normalized light intensities of the microlenses at different focal lengths were measured and matched well with a Zemax light-ray tracing simulation. The hydrogel durability was also tested.

## 2. Mechanism and structures

Figure 1(*a*) shows the schematic of a 4 × 4 microlens array. Each liquid-based tunable-focus microlens in the microlens array is actuated by a thermo-responsive hydrogel microstructure, reported in the previous articles [12, 15]. The 3D cross-sectional view of one microlens is shown in figure 1(*b*). The microlens is formed by a curved immiscible liquid–liquid interface which is pinned by a treated hydrophobic–hydrophilic (H–H) boundary at the top edge of an aperture. Deionized water and silicone oil are used here and are constrained in a water container and an oil container, respectively. The water container, the oil container and the aperture layer between two containers are all made of a flexible polymer. Oil prevents the evaporation of water and serves as the lens material along with water since the refractive index of oil ($n_1 = 1.48$) is larger than that of water ($n_2 = 1.33$). Various hydrogel microstructures located in the water container respond to the change in the local temperature, absorbing and releasing water in the water container and expanding and contracting their volume at low/high temperature, respectively. The net volumetric change in water regulates the pressure difference across the water–oil interfacial meniscus. The meniscus bulges downward with the contracted hydrogels and protrudes upward with the expanded ones, varying its radius of curvature and consequently the focal length of the microlens.

## 3. Spherical aberrations of microlenses

### 3.1. Physical model

The aberration is one of many possible ways to characterize the quality of an optical imaging system [18]. Spherical aberrations of lenses occur because the refraction of light rays near the edge of a lens is stronger than that near the center of the lens. The spherical aberration depends on the ray position in the exit pupil but is independent of the position in the image plane [19]. Here we present a simple model to describe the microlens spherical aberrations.

The geometry of a microlens is shown in figure 2. The microlens is formed through the interface between deionized water and silicone oil. Their refractive indices are $n_2 = 1.33$ and $n_1 = 1.48$, respectively. The microlens diameter, $d$, is a constant. The radius of curvature of the water–oil interface, $R$, varies with the pressure in the water container. $O$ is the center of the interface curvature. $\theta_i$, $\theta_t$ and $\alpha$ are the incident angle, the refracted angle and the difference between two angles, respectively. The microlens focal length, $f$, equals

$$f = \frac{R}{n_1 - n_2} \tag{1}$$

and the $x$ axis is in the microlens focal plane. Two refracted light rays from the center and edge of the microlens intersect at the point of $O'$. The distance between the intersection point $O'$ and the focal plane is $\Delta Z$, called the longitudinal spherical aberration [19]. The light ray from the edge of the microlens strikes the focal plane at the point $A$. The distance from the point $A$ to the optical axis $OO'$ is $\varepsilon_x$, called the transverse spherical aberration [19].

$$\varepsilon_x = \Delta Z \cdot \tan\alpha = \frac{d}{2} - (f + R\,(1 - \cos\theta_i)) \cdot \tan\alpha, \tag{2}$$

where

$$\alpha = \theta_t - \theta_i \tag{3}$$

and

$$n_1 \cdot \sin\theta_i = n_2 \cdot \sin\theta_t. \tag{4}$$

The calculated result is shown in section 5.7.

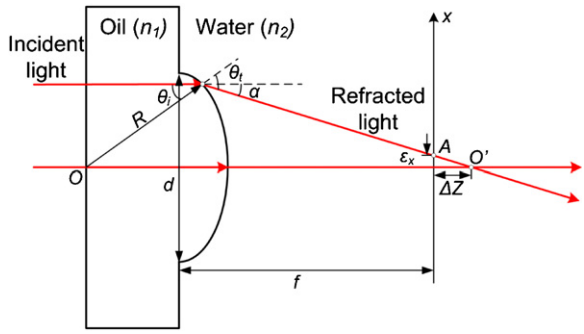


**Figure 2.** Schematic of the physical geometry of a microlens. The microlens is formed through a liquid–liquid interface. The longitudinal spherical aberration is the difference between the focal length calculated from equation (1) and the intersection point of the real light rays, $O'$. The transverse spherical aberration is the projection of the longitudinal spherical aberration on the focal plane.

### *3.2. Light-ray tracing simulation*

The light propagation in the microlens and the surrounding environment was simulated using Zemax, a light-ray tracing software program (Zemax EE, ZEMAX Development Corporation, Bellevue, WA, USA) [20]. The liquid–liquid interface is assumed to be spherical because of the small difference of mass density of deionized water and silicone oil [8]. The refractive index of deionized water and silicone oil are assumed to be 1.33 and 1.48, respectively, independent of the wavelength. The simulation results are also presented in section 5.7.

## 4. Fabrication processes

The fabrication method of the microlens array was based on liquid phase photopolymerization, called $LP^3$ [21, 22] and soft lithography [23]. First, the molds were formed through $LP^3$ and then the mold structures were transferred to a flexible polymer, polydimethylsiloxane (PDMS), through soft lithography to form the structure of the microlens array. Benefitting the flexibility of polymeric PDMS, the microlens array was suitable for flexible devices and can be used potentially for curvilinear surfaces [17].

### *4.1. Polymer precursors*

Several polymers were used to construct the structure of the microlens array. The molds were made of poly isobornyl acrylate (IBA), which could be patterned under ultraviolet (UV) light. PDMS transferred from the molds was used to form the polymer containers for deionized water and silicone oil. The recipes of poly-IBA and PDMS have been previously reported [20].

Structure- and size-varied thermo-responsive hydrogels were formed in the water container to actuate the microlenses. *N*-isopropylacrylamide (NIPAAm) hydrogels are thermo-responsive and exhibit a reversible volumetric change depending on the local temperature. At low temperature, they expand and absorb water, while at high temperature, they shrink and release water. NIPAAm hydrogel pre-polymer solutions consist of five components [21, 22]: 0.545 g NIPAAm as the monomer, 0.0385 g 2,2-dimethoxy-2-phenylace-tophenone (DMPA) as the co-monomer, 0.031 g *N*,*N*′-methylenebisacrylamide (NMBA) as the cross-linker, 0.75 mL dimethyl sulfoxide (DMSO) and 0.25 mL gold deionized water as the solvents. All chemicals were supplied by Acros Organics (Morris Plains, NJ, USA) and were used without alteration.

NIPAAm hydrogels begin to contract when the temperature increases from lower than to above the lower critical solution temperature (LCST) of NIPAAm hydrogel [24]. A small amount of an ionizable monomer, 3-(methacryloylamino) propyl trimethylammonium chloride (MAPTAC) was added into the hydrogel pre-polymer solutions to increase the LCST of NIPAAm hydrogels [13, 25]. Two concentrations of MAPTAC, 0.15% volume/volume (V/V) and 0.3% V/V, were mixed into the hydrogel solutions and the LCST shifted from 32 to 42 °C and 48 °C, respectively. They are called MAPTAC I and MAPTAC II hydrogels in this paper, respectively.

### *4.2. Fabrication process flow*

Figure 3 shows the fabrication process flow of the microlens array. The whole structure was formed by bonding three layers of PDMS structure together: the water container, aperture slip and oil container. First, a chamber was formed on a glass slide by two layers of adhesive tape (3M Adhesive Transfer Tape 467MP, 3M Corporate, St. Paul, MN) and was filled with an isobornyl acrylate (IBA) pre-polymer solution. The thickness of each layer of adhesive tape is 250 $\mu$m. The cavity was 500 $\mu$m thick. A film photomask (Mask-1) was aligned on top of the chamber to form a poly-IBA cylinder structure in the chamber under UV radiance (intensity, $I_{UV}$ = 8.0 mW cm$^{-2}$; time, $t$ = 100 s), as shown in figure 3(*a*). UV radiance was provided by a desktop EXFO Acticure 4000 (EXFO Photonic Solutions, Inc., Missisauge, ON, Canada) UV light source. All photomasks were 3000 dots per inch (dpi) and were printed on transparent films by Imagesetter Inc. (Madison, WI, USA).

The unexposed poly-IBA solution was flushed away with ethanol. Figure 3(*b*) shows the patterned poly-IBA structure on the glass slide. This was a mold for PDMS transfer. In order to reduce the adhesion between PDMS and the poly-IBA mold when separating PDMS from the poly-IBA mold, the surface of the mold was evaporated with a layer of releasing agent tridecafluoro-1,1,2,2-tetrahydrooctyl trichlorosilane (Gelest Inc., Morrisville, PA) in vacuum for 1 h.

Then, another three layers of 3M adhesive tape were applied around the patterned structure on the glass slide, forming a 750 $\mu$m thick chamber. The PDMS pre-cured solution was filled into the chamber from the top and was cured at 70 °C for 8 h for polymerization. The shape of poly-IBA molds was, therefore, transferred to the cured PDMS structure, as shown in figure 3(*c*).

Next, the cured PDMS structure was peeled off of the mold for the water container. The surface of the PDMS structure

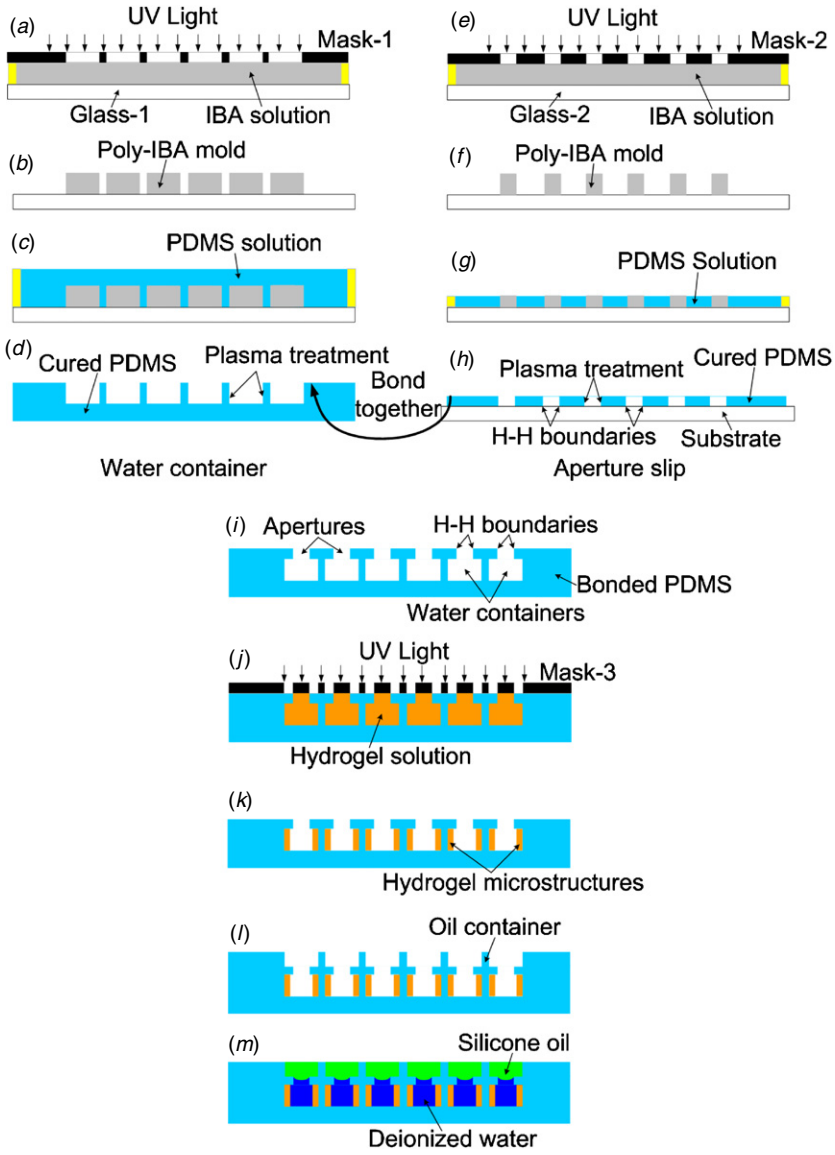


**Figure 3.** Fabrication process flow of a liquid-based tunable-focus microlens array actuated by the thermo-responsive NIPAAm hydrogel microstructures. The whole process is based on $LP^3$ and soft lithography. (*a*) A chamber confined by two layers of 3M adhesive transfer tape was filled with the IBA pre-polymer solution. The thickness of the chamber was 500 $\mu$m. The poly-IBA structures were patterned in the chamber under UV radiance (intensity, $I_{UV} = 8.0$ mW cm$^{-2}$; time, $t = 100$ s). (*b*) The chamber was then rinsed with ethanol and the unexposed solution was removed. The poly-IBA structures for the mold were formed on the glass substrate. In order to reduce the adhesion between PDMS and the mold, the surface of the mold was evaporated with a layer of releasing agent to be more hydrophobic. (*c*) Another three layers of 3M adhesive tape were used to form a chamber around the patterned structures with the thickness of 750 $\mu$m. The PDMS pre-cured solution was filled into the chamber and then cured at 70 °C for 8 h. (*d*) The PDMS polymer structure was peeled off of the poly-IBA mold. The top surface of the PDMS layer was treated to be hydrophilic by corona discharge plasma. (*e*) and (*f*) Similar procedures were carried out to form a 250 $\mu$m thick poly-IBA mold on a glass slide. (*g*) The PDMS pre-polymer solution was poured into the chamber. The surface of the solution was level with the mold. The extra solution was removed with a razor and then was cured at 70 °C for 8 h. (*h*) The PDMS aperture slip was peeled off the mold and was placed on a polystyrene substrate. The top surface and the sidewall of the apertures were treated to be hydrophilic by corona discharge plasma and the bottom surface was kept hydrophobic because of the protection of the substrate, forming a H–H boundary. (*i*) The two PDMS layers were bonded together using the treated surfaces, forming the water container. (*j*) The water containers were filled with the NIPAAm hydrogel pre-polymer solution and then were photopatterned under UV radiance ($I = 13.5$ mW cm$^{-2}$; $t = 14$ s). (*k*) The unexposed hydrogel solution was washed away with ethanol and the hydrogel rings were formed in each water container. (*l*) Similar procedures were carried out to fabricate a PDMS layer for the oil container. This fabrication process is not shown here. This layer was then bonded on the top of the aperture slip, forming the oil containers. (*m*) The containers were filled with deionized water and silicon oil consecutively, forming the immiscible water–oil interfaces for the microlenses.

was treated to be hydrophilic by corona discharge plasma (BD-20, Electro-Technic Products Inc., Chicago, IL) [26, 27], as shown in figure 3(*d*). Section 5.1 shows the result of the surface treatment.

A similar procedure was carried out to fabricate another PDMS structure for the aperture slip, as shown in figures 3(*e*)–(*h*). The thickness of the poly-IBA mold in figure 3(*f*) was 250 $\mu$m. In order to form the through-holes, the height of the

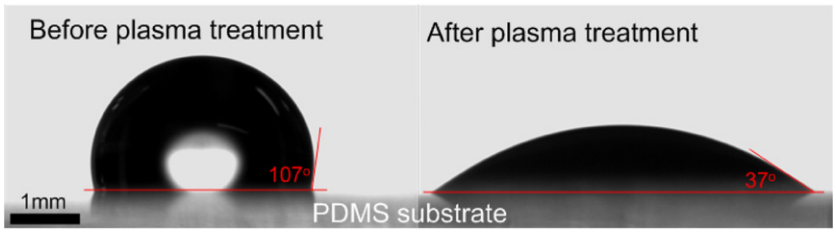


**Figure 4.** Pictures of the side profile of deionized water on the surfaces of PDMS before and after the corona discharge plasma treatment. After the treatment, the PDMS surface changed from hydrophobic to hydrophilic and the corresponding contact angle of deionized water reduced from 107° to 37°.

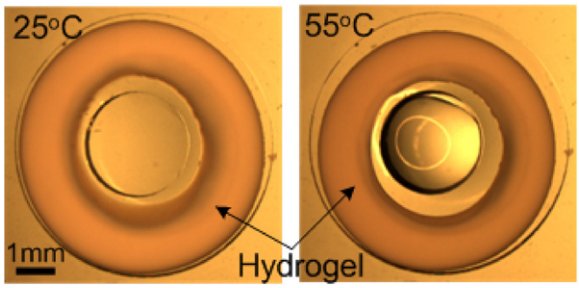


**Figure 5.** Pictures of a thermo-responsive hydrogel ring in deionized water taken from above. The hydrogel volume changes responsive to the local temperature. From room temperature (25 °C) to 55 °C, the hydrogel ring released water and its volume shrank to 83.9% of the original.

PDMS pre-cured solution was the same as that of the mold, as shown in figure 3(*g*). The extra PDMS solution above the top surface of the mold was removed with a razor. Next the PDMS was cured at 70 °C for 8 h for polymerization.

The PDMS aperture slip was peeled off of the mold and placed on a polystyrene disposable Petri dish (Fisher Scientific, 2000 Park Lane Drive, Pittsburgh, PA, USA), as shown in figure 3(*h*). The top surface and sidewall of the aperture slip were then treated to be hydrophilic by corona discharge plasma. Owing to the protection of the polystyrene substrate, the bottom surface of the aperture slip was still hydrophobic, forming the H–H boundary at the edge of the apertures, as shown in figure 3(*h*).

These two treated hydrophilic surfaces of the two PDMS layers were bonded together by applying a pressure, forming the water container, as shown in figure 3(*i*). The layers were manually aligned under a stereomicroscope (Nikon SMZ1500, Nikon Instruments, Inc., Melville, NY, USA). The H–H boundary was at the top edge of each aperture.

Then, the water containers were filled with the thermo-responsive NIPAAm hydrogel pre-polymer solution and a film photomask (Mask-3) was manually aligned on top of the water containers, as shown in figure 3(*j*). Under UV radiance ($I = 13.5$ mW cm$^{-2}$; $t = 14$ s), a hydrogel ring was formed in each water container, as shown in figure 3(*k*). The unexposed hydrogel solution was removed with ethanol.

Finally, a third PDMS layer for the oil container was formed by using the same procedure as that of the aperture slip, not shown here. It was 300 $\mu$m thick. After the surface treatment, this PDMS layer was manually aligned to and bonded on the top of the aperture slip, forming the oil containers, as shown in figure 3(*l*). Finally, deionized water was filled into the water chamber and silicone oil was filled into the chamber to cover water, forming the microlenses, as shown in figure 3(*m*). Limited from the size variation of the microlens and hydrogel structures and the water absorption of hydrogels [28], the volume of deionized water in each water container varied and therefore the tuning range of the focal length of the microlenses were different. More details are presented in section 5.4.

## 5. Experimental results

### *5.1. Contact angle measurement*

Surfaces of polymeric PDMS are intrinsically hydrophobic and can be rendered hydrophilic after the corona discharge plasma treatment [26, 27]. The surface energy of a solid surface is defined by a contact angle between a liquid and the solid surface [29]. A deionized water droplet was placed on the surface of PDMS before and after the corona discharge plasma treatment. The droplet contact angles on the PDMS surfaces were measured by a goniometer (OCA 15+, DataPhysics Instruments, Inc., Germany). Figure 4 shows pictures of deionized water from the side on the PDMS surfaces before and after the corona discharge plasma treatment. The PDMS surface was naturally hydrophobic and the contact angle of deionized water on it was measured to be 107°. After the corona discharge plasma treatment, the surface was changed from hydrophobic to hydrophilic and the contact angle of deionized water was reduced to 37°.

### *5.2. Volumetric change in the hydrogel*

Figure 5 shows pictures of a thermo-responsive NIPAAm hydrogel ring at two different temperatures. The images were taken by the Nikon stereomicroscope from the top. The hydrogel ring was photopatterned in a cavity filled with deionized water. When the environmental temperature increases from room temperature (25 °C) to 55 °C, the hydrogel releases water and contracts. The procedure is reversible. As the temperature decreases, the hydrogel ring absorbs water and expands to the original shape. Because of the constraint from the top and bottom plates, the height change in the hydrogel ring was negligible. The area of the hydrogel ring was calculated from the images in figure 5 by using ImageJ [30]. Compared with the original status at room temperature, the volume of the contracted hydrogel at high temperature shrank to 83.9%.

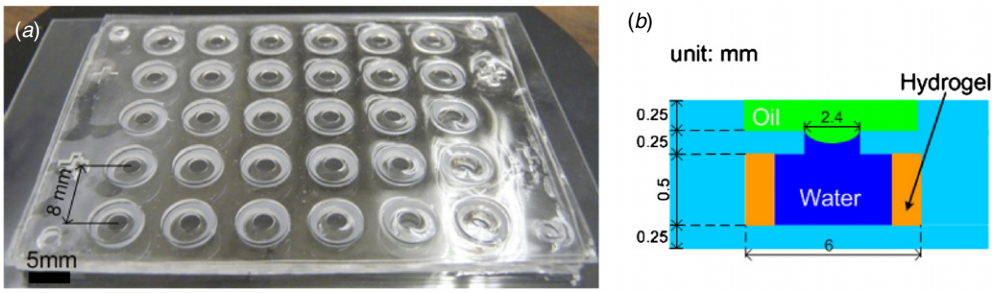


**Figure 6.** (*a*) Optical image of the structure of one PDMS microlens array without the lens liquids. The array consisted of 5 × 6 microlens structures. The picture was taken by a camera from an oblique angle. (*b*) Cross-sectional schematic of one microlens and its size specifications.

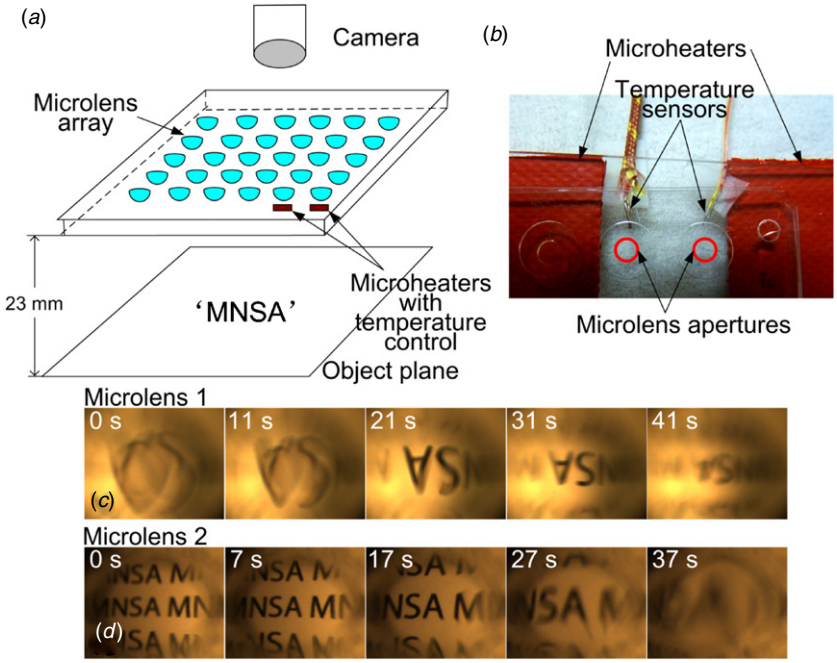


**Figure 7.** (*a*) Schematic of the setup to form images on a camera through the microlens array. An object plane ('MNSA') was placed 23 mm below the microlens array and a camera-coupled stereomicroscope was used to monitor and record images from the microlenses. Two resistive microheaters were placed under the microlenses and were connected to an individual temperature controller. (*b*) Image of the two microlenses with the corresponding microheater and the temperature sensor under the microlenses. (*c*) Frame sequence of the images obtained from the microlens 1. The images from the microlens 1 were inverted, enlarged and real. At the time instant of 21 s, the image was clear and sharp. (*d*) Frame sequence of the images obtained from the microlens 2. The images from the microlens 2 were erect, enlarged and virtual. At the time instant of 17 s, the image was clear and sharp. After the time instant of 27 s, the images became blurred.

### *5.3. Images from the microlens array*

Figure 6(*a*) shows an optical image of one 5 × 6 microlens array before filling the lens liquids. The image was taken by a Canon EOS 40D camera with a Canon EF 17–40 mm f/4.0 L USM lens (Canon USA, Inc., Lake Success, NY, USA) from an oblique angle. The center distance between any two microlenses is 8 mm. The size details of each microlens are illustrated in figure 6(*b*). The diameter of each microlens aperture is 2.4 mm. The diameters of the water container and the oil container are the same to be 6 mm. The heights of two containers are 250 $\mu$m and 500 $\mu$m, respectively. The thicknesses of both the aperture slip and the bottom of the water container are 250 $\mu$m.

Figure 7(*a*) shows the setup to form images on a camera through the microlens array with 5 × 6 microlenses. Each microlens in the array could be actuated individually by controlling the local temperature. An object plane with a logo 'MNSA' was placed 23 mm below the microlens array and images through the microlenses were monitored and recorded by the camera-coupled Nikon stereomicroscope. Two resistive microheaters (SRFG-102J, OMEGA Engineering, Inc., Stamford, CT, USA) were placed under the microlens array and each microheater was connected to an individual temperature controller (CSC32 Benchtop, OMEGA Engineering, Inc., Stamford, CT, USA). Figure 7(*b*) was taken from the top and shows two microlenses with the corresponding microheaters and the temperature sensors.

Figures 7(*c*) and (*d*) show the image frame sequence through two microlenses in the array, respectively. Initially, the focal length of the microlens 1 was less than 23 mm and the distance from the microlens to the object plane was between

one and two times of the focal length. The image was inverted, enlarged and real, as shown in figure 7(*c*). As temperature increased, the focal length of the microlens decreased and the size of the images shrunk. At the time instant of 21 s, the microlens formed a clear image on the camera of the stereomicroscope.

For the microlens 2, the original focal length was larger than the distance from the microlens to the object plane of 23 mm. The image was erect, enlarged and virtual, as shown in figure 7(*d*). When the focal length of the microlens decreased, the size of the virtual image enlarged. At the time instant of 17 s, the image was clear and sharp. After the time instant of 27 s, the camera was out of the image plane and the images became blurred.

### 5.4. Focal length measurement

The microlens array was mounted on and was moved by a 3D translation stage (Parker Hannifin Corporation, Cleveland, OH, USA). The temperature around the microlenses was controlled in the range from 24 to 60 °C, as described in section 5.3. The temperature was recorded by a digital thermometer (HH506RA, OMEGA Engineering, Inc., Stamford, CT, USA). Collimated light at a wavelength of 633 nm from a laser (JDS Uniphase 1107, JDS Uniphase Corporation, Santa Rosa, CA, USA) illuminated the microlens array from the bottom. A microscope (The Microscope Store, L.L.C., Wirtz, VA, USA) was focused on the top surfaces surrounding the microlenses using as the zero point. At a specific temperature, the stage was moved along the optical axis to the focal point by finding the minimum laser spot in the microscope. This distance, from the zero point to the focal point, was the microlens focal length [20].

In theory, the microlens focal length is contributed from the water–oil interface and the top oil surface. The top oil surface is not completely flat because of the surface tension. The microlens structure was filled with oil and the focal length of the top oil surface was measured by using the above method. The focal length was approximately 800 mm. Compared with the variable range of the focal length in tens of millimeters, the focal length of the top oil surface can be neglected and this surface is treated flat in our experiments.

Figure 8 shows the focal length as a function of the temperature of four microlenses with various initial volume of deionized water. Microlenses 1 and 2 are discussed in section 5.3. With increasing temperature, the microlens focal length decreased. These microlenses showed different initial focal lengths and focal length ranges. By controlling the initial volume of deionized water filled in the water container, the microlenses could be set in different tuning ranges of the focal length and could be tuned individually in that specified focal length range.

### 5.5. Effect of the hydrogel shape on response times

Here we show another method to dynamically measure the microlens focal length as a function of time. Figure 9 shows the mechanism to measure the microlens focal length with time. Collimated incident light at the wavelength of 633 nm

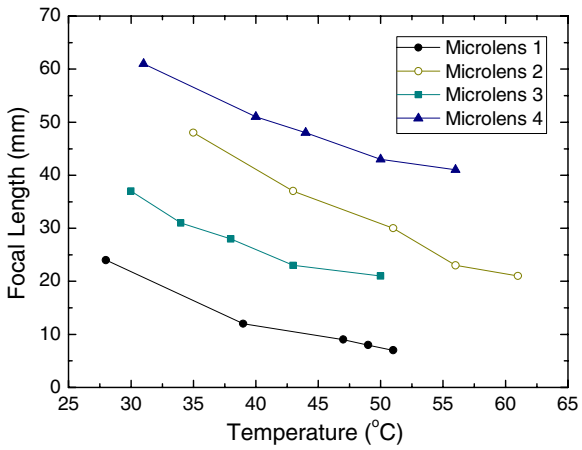


**Figure 8.** Focal length as a function of temperature of four microlenses in a microlens array. The initial focal length at room temperature and the tuning range of the focal length can be varied, depending on the initial volume of water filled in the water container. The focal length decreased with increasing temperature.

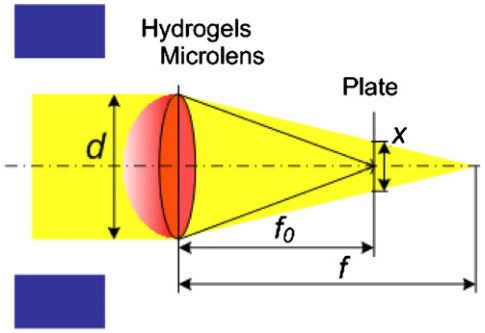


**Figure 9.** Schematic of the set-up to dynamically measure the focal length of a microlens. An incident light from a collimated laser illuminates a microlens from the bottom. The diameter of the microlens, namely that of the incident light, is *d*. A semitransparent plate is moved along the optical axis of the microlens by a translation stage. When the focal length of the microlens is tuned to the minimum, the plate is moved to the focal point by finding the minimum spot of the focused laser light. The distance between this point and the microlens is $f_0$. When the focal length of the microlens increases, the focal point moves to the back of the plate and thus the size of the spot on the plate increases. The diameter of the spot is measured to be *x*. The dynamic focal length of the microlens can be calculated from equation (5).

from the laser illuminates the microlens from the bottom. The diameter of the microlens is *d*. A semitransparent plate is placed on the translation stage and moves along the microlens optical axis. At high temperature (55 °C), when the hydrogel is most contracted and the microlens focal length is tuned to the minimum, the plate is moved to the focal point by finding the sharpest spot of the incident laser light. The distance between this point and the microlens is $f_0$, as shown in figure 9. The solid lines in figure 9 show the incident light rays when the microlens focal length is minimum. With increasing focal length, the focal point moves to the back of the plate and thus the spot size on the plate increases and is measured to

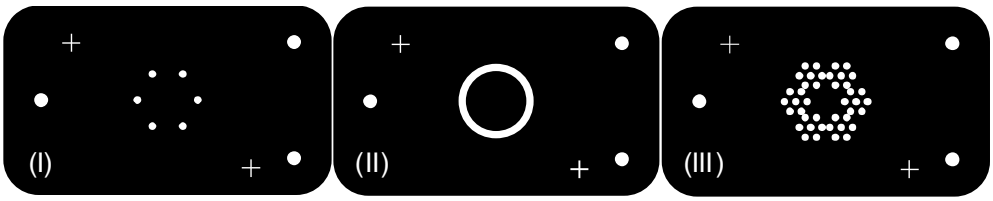


**Figure 10.** Masks to pattern hydrogel microstructures in the water container. In pattern I, there are six hydrogel posts distributed on a circle of 8 mm diameter. The diameter of each post is 1 mm. In pattern II, there is a ring whose inner and outer diameters are 8 mm and 9 mm, respectively. In pattern III, there are six groups of hydrogel posts and seven hydrogel posts in each group. The diameter of each post is 1 mm. The center posts in each group are distributed on a circle of 8 mm diameter. The total surface areas of patterns I, II and III are 9.43, 26.70 and 65.97 mm$^2$, respectively, without considering the deformation of the hydrogel microstructures during the temperature change.

be $x$. Therefore, the dynamic microlens focal length could be calculated by equation (5):

$$f = f_0 \frac{d}{d - x}. \tag{5}$$

Compared to the method in section 5.4, this method does not require moving the microlenses during the measurement and can provide continual measurement of the focal length. However, because the aberrations of microlenses exist and vary with the focal length, the focal point cannot focus on a fine spot and thus the error should be larger than the previous method.

The effect of the hydrogel microstructure shape on the microlens response time was compared. Here, in order to fabricate more complicated hydrogel microstructures in the water container, the diameter of the water container increases to 10 mm and the others keep the same. Masks used to pattern the hydrogel microstructures are shown in figure 10. There are three patterns of the hydrogel microstructures. In pattern I, there are six hydrogel posts distributed on a circle of 8 mm diameter. The diameter of each post is 1 mm. In pattern II, there is a ring whose inner and outer diameters are 8 mm and 9 mm, respectively. In pattern III, there are six groups of the patterns. In each pattern, there are seven posts of 1 mm diameter and the center posts are distributed on a circle of 8 mm diameter. In total there are 42 hydrogel posts. The side surface areas of three patterns are calculated without the consideration of the deformation of the hydrogel microstructures during the temperature change and to be 9.43, 26.70 and 65.97 mm$^2$, respectively.

When the microlenses were tested, the environmental temperature around the microlenses increased to 60 °C and then decreased to room temperature (25 °C) by natural dissipation. Spot images on the plate were recorded by an industrial charge-coupled device (CCD) camera (AVT Stingray IEEE1394 C-Mount Cameras, Allied Vision Technologies GmbH, Germany) and then the dynamic microlens focal length changes with time could be calculated, as shown in figure 11. The triangle, square and circle curves are the dynamic focal length change with time of the microlens actuated by the hydrogel microstructures patterned by patterns I, II and III in figure 10, respectively.

Of the three hydrogel microstructures, the pattern III structure had the fastest response time, which was 20 s for a full cycle. The pattern I structure had the slowest response time with a full cycle of around 1.5 min. The full cycle of

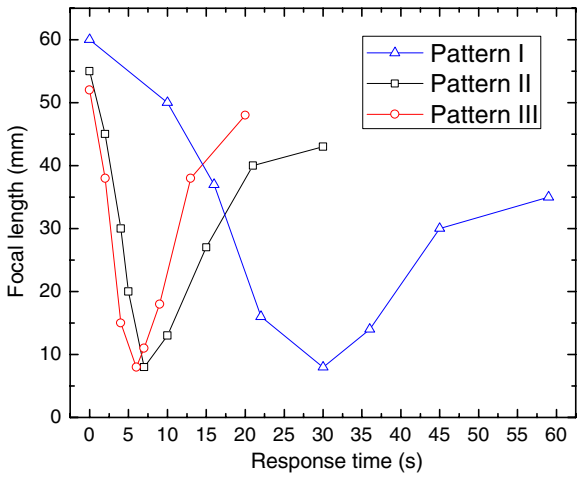


**Figure 11.** Dynamic focal length change with time of the microlenses actuated by the hydrogel microstructures patterned by pattern I, pattern II and pattern III in figure 10, respectively.

the microlens actuated by the pattern I structure is shown in figure 12. The response time of microlenses is relative to the diffusion time of the hydrogels, proportional to the total surface area. The total surface area of the pattern III structure was much larger than that of the pattern I structure and the corresponding response time is faster. With an increased surface area of the hydrogel microstructures, the microlens response time could be improved further.

### *5.6. Effect of the hydrogel LCST on response times*

Here the effect of the hydrogel LCST on the microlens response time was also compared. Three types of hydrogels with different LCSTs, NIPAAm, MAPTAC I and MAPTAC II, were patterned in the water container by using the pattern I mask to actuate the microlenses. The microlenses had the same parameters as before. The dynamic microlens focal length change with time actuated by the three types of hydrogels is shown in figure 12. The square, circle and triangle curves are the dynamic microlens focal length change with time actuated by the NIPAAm, MAPTAC I and MAPTAC II hydrogel microstructures, respectively. Because of the higher LCST, when the temperature rises, the microlenses is tuned slower, but when the temperature falls, the microlens response time is faster. The microlens actuated by the MAPTAC II hydrogel microstructures had the smallest gap between the rising time

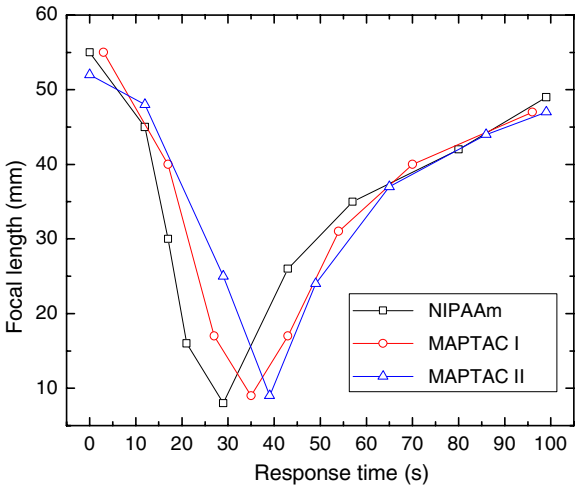


**Figure 12.** Dynamic focal length change with time of the microlenses actuated by three types of hydrogels. All microlenses were actuated by the hydrogel microstructure patterned by the pattern I mask in figure 10. The square, circle and triangle curves are the dynamic focal length change with time of the microlenses actuated by the NIPAAm, MAPTAC I and MAPTAC II hydrogel microstructures, respectively. The microlens actuated by the NIPAAm hydrogel microstructures had the largest gap between the rising time and the falling time.

and the falling time. Therefore, the microlens response time could be increased by increasing the NIPAAm hydrogel LCST.

### *5.7. Spherical aberration*

The transverse spherical aberration of a microlens was calculated from equations (2)–(4), as plotted in figure 13. Here the diameter of the microlens was a constant, 2.4 mm. The focal length, $f$, varied from 8.9 to 80 mm. The corresponding incident angle, $\theta_i$, calculated from the focal length and the microlens aperture in figure 2, varied from 63° to 5.5°. The calculated transverse spherical aberration, $\varepsilon_x$, was from −450 to 260 $\mu$m and equaled zero when the focal length was 11.5 mm.

Collimated light at a different wavelength of 473 nm from a blue laser (DPSS Laser System, Laserglow Technologies, Toronto, Canada) illuminated a typical microlens in the microlens array from the bottom, as described in section 5.4. The AVT Stingray camera was mounted on the translation stage and was moved along the microlens optical axis to the focal point. The camera resolution was 640 × 480 pixels and the size of each pixel was 8.3 × 8.3 $\mu$m$^2$. The focused spot images at three focal lengths and the laser spot at the distance of 25 mm were recorded by the CCD in the camera, as shown in figure 13. The laser spot was formed through the microlens structure without any lens liquids. The normalized light intensities were extracted from the images and were plotted as circle spots in figure 14.

The light intensity profiles at three microlens focal length were simulated by Zemax. Point spread function (PSF) analysis was performed in Zemax for the microlens, as shown as the black solid line in figure 14. From figures 14(*a*)–(*c*), the distribution of light intensities at three microlens focal

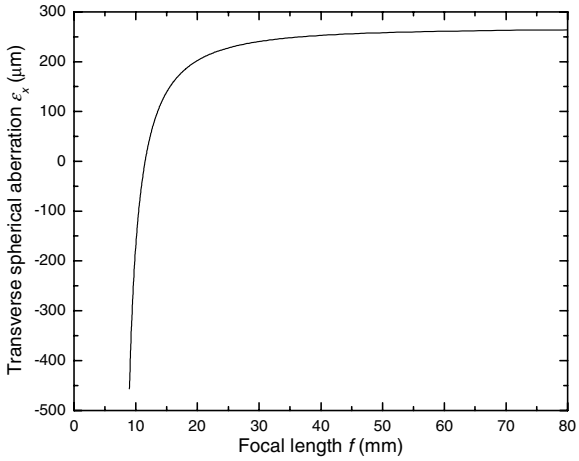


**Figure 13.** Relationship between the transverse spherical aberration, $\varepsilon_x$, and the focal length, $f$, of the microlenses. The calculated transverse spherical aberration equals zero when the focal length was 11.5 mm.

length extracted from the images matched well with the Zemax simulation. Figure 14(*d*) shows the light intensity of the laser spot at the distance of 25 mm without any lens liquids. Because of the diffraction of the polymer material, the curve in figure 14(*d*) is not smooth.

Normally the spherical aberrations from normalized light intensities are defined as the full width at half maximum (FWHM). In order to compare with the calculated transverse spherical aberrations, however, we define the spherical aberrations from the normalized light intensities as the width at minimum. The spherical aberrations at the focal length of 25 mm, 41 mm and 71 mm were 58 $\mu$m, 166 $\mu$m and 290 $\mu$m, respectively. The spherical aberrations from the normalized light intensities had a good match with that calculated from equations (2)–(4).

### *5.8. Durability*

In order to measure the hydrogel durability, a serial of round hydrogel microstructures were tested in deionized water. They were heated up for contraction and cooled down for expansion for 300 cycles. In each cycle, the temperature around the round hydrogel microstructure was increased to 75 °C for 10 s and then was cooled down to room temperature for 1 min. The whole testing procedure was finished in 48 h. After 300 cycles, the hydrogel microstructure could still respond to the temperature change. However, the water container was broken, halting further testing of the hydrogel response. A better water container will be fabricated in the future and the testing cycle will be increased to the hydrogel limit.

## 6. Summary

In summary, we have presented a microlens array consisting of liquid-based tunable-focus microlenses which can be individually actuated by thermo-responsive hydrogel microstructures and respond to the environmental temperature. The microlenses are formed through the curved water–oil

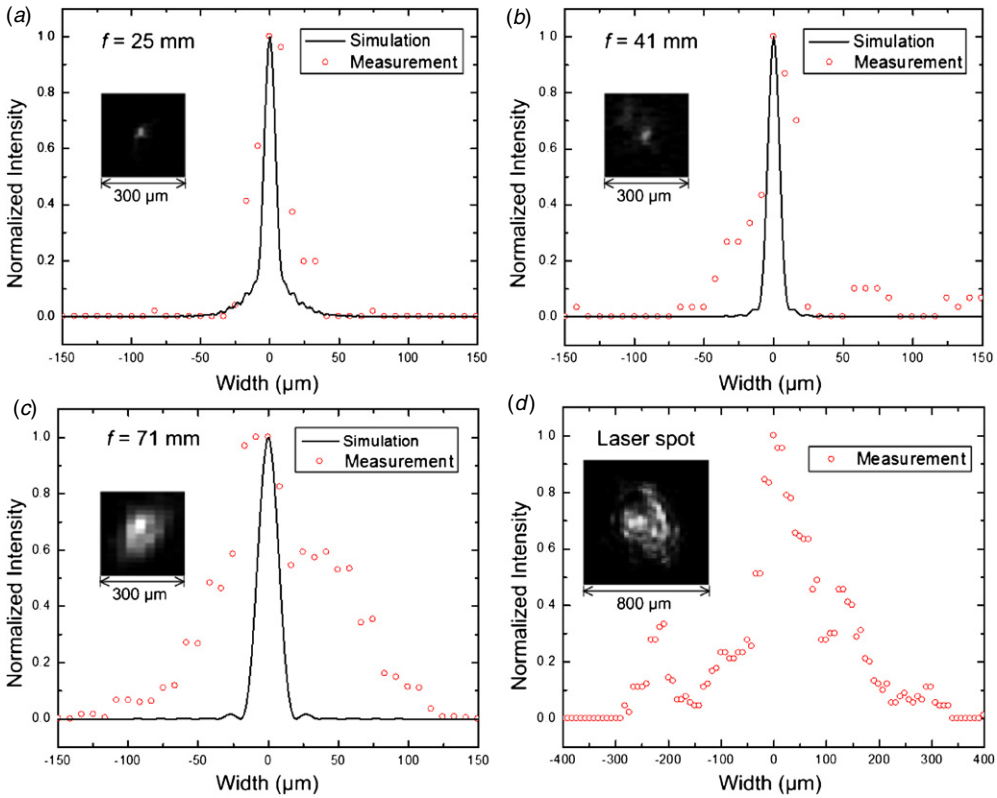


**Figure 14.** Normalized light intensities of the focused spots of one typical microlens at the focal length of (*a*) 25 mm; (*b*) 41 mm and (*c*) 71 mm. The circle curves were extracted from the images taken by a camera at the focal point. The simulation result using the light-ray tracing software, Zemax, is the solid curves. (*d*) Normalized light intensity of the laser spot at the distance of 25 mm without any lens liquids.

interfacial meniscus. The net volumetric change in the hydrogels and deionized water regulates the pressure across the interface and varies the microlens focal length. The microlenses are 2.4 mm in diameter. The microlens focal length was measured by two methods. Their focal length varied from around 60 to around 8 mm and the response time for the full cycle varied from 20 s to 1.5 minute depending on the patterns of the actuation hydrogel microstructures. A large surface area of the hydrogel microstructures can decrease the response time. The hydrogel with the higher LCST can also be used to decrease the microlens response time. The normalized light intensities of the microlenses at different focal lengths were measured and matched well with that from the Zemax light-ray tracing simulation. The spherical aberrations from the light intensities had a good match with the theoretical results. The hydrogel durability was also tested.

In the future, the microlens response time could be improved by increasing the total surface area and the hydrogel LCST. The effect of the liquid-based microlens shape on optical performance, especially on spherical aberrations, could be reduced or even eliminated by studying and optimizing the pressure distribution, gravity and these corresponding interface shapes. The relationship of the water volume, the temperature change and the range of the focal length will be studied with the characterization of the water absorption of hydrogels. The hydrogel durability will also be tested to define their lifetime. Benefitting from the flexible polymers in the microlens structure, the microlenses will be fabricated and tested on some curvilinear surfaces for the improvement of optical performance [31] and flexible application.

## Acknowledgment

This work was supported by the US National Science Foundation (ECCS 0702095 and ECCS 0745000), the Wisconsin Institutes for Discovery, and the Wallace H. Coulter Foundation. The authors thank Bader Aldalali, Kevin Eliceiri and Gunnsteinn Hall for their discussions and assistance.

## References

[1] Jiang H and Dong L 2006 Smart lenses *Phys. World* **19** 29–31
[2] Jeong K H *et al* 2004 Tunable microdoublet lens array *Opt. Express* **12** 2494–500
[3] Zhang D Y *et al* 2003 Fluidic adaptive lens with high focal length tunability *Appl. Phys. Lett.* **82** 3171–2
[4] Ren H and Wu S T 2005 Variable-focus liquid lens by changing aperture *Appl. Phys. Lett.* **86** 211107
[5] Lee S W and Lee S S 2007 Focal tunable liquid lens integrated with an electromagnetic actuator *Appl. Phys. Lett.* **90** 121129
[6] Lopez C A, Lee C C and Hirsa A H 2005 Electrochemically activated adaptive liquid lens *Appl. Phys. Lett.* **87** 134102
[7] Yang S *et al* 2003 Tunable and latchable liquid microlens with photopolymerizable components *Adv. Mater.* **15** 940–3
[8] Kuiper S and Hendriks B H W 2004 Variable-focus liquid lens for miniature cameras *Appl. Phys. Lett.* **85** 1128–30
[9] Gorman C B, Biebuyck H A and Whitesides G M 1995 Control of the shape of liquid lenses on a modified gold

surface using an applied electrical potential across a self-assembled monolayer *Langmuir* **11** 2242–6
[10] Cheng C C and Yeh J A 2007 Dielectrically actuated liquid lens *Opt. Express* **15** 7140–5
[11] Ren H and Wu S T 2008 Tunable-focus liquid microlens array using dielectrophoretic effect *Opt. Express* **16** 2646–52
[12] Dong L *et al* 2006 Adaptive liquid microlenses activated by stimuli-responsive hydrogels *Nature* **442** 551–4
[13] Dong L *et al* 2007 Variable-focus liquid microlenses and microlens arrays actuated by thermoresponsive hydrogels *Adv. Mater.* **19** 401–5
[14] Dong L and Jiang H 2007 Tunable and movable liquid microlens *in situ* fabricated within microfluidic channels *Appl. Phys. Lett.* **91** 041109
[15] Zeng X and Jiang H 2008 Tunable liquid microlens actuated by infrared light-responsive hydrogel *Appl. Phys. Lett.* **93** 151101
[16] Osada Y, Gong J P and Tanaka Y 2004 Polymer gels (Reprinted from Funct. Monom. Polym. 497–528 1997) *J. Macromol. Sci. Polym. Rev.* C **44** 87–112
[17] Zhu D F *et al* 2010 Tunable-focus microlens arrays on curved surfaces *Appl. Phys. Lett.* **96** 081111
[18] Scott C 1998 *Introduction to Optics and Optical Imaging* (New York: Wiley)
[19] Guenther R 1990 *Modern Optics* (Cambridge: Wiley)
[20] Zeng X and Jiang H 2008 Polydimethylsiloxane microlens arrays fabricated through liquid-phase photopolymerization and molding *J. Microelectromech. Syst.* **17** 1210–7
[21] Agarwal A K, Beebe D J and Jiang H 2006 Integration of polymer and metal microstructures using liquid-phase photopolymerization *J. Micromech. Microeng.* **16** 332–40
[22] Beebe D J *et al* 2000 Microfluidic tectonics: a comprehensive construction platform for microfluidic systems *Proc. Natl Acad. Sci. USA* **97** 13488–93
[23] Xia Y N and Whitesides G M 1998 Soft lithography *Annu. Rev. Mater. Sci.* **28** 153–84
[24] Wang J *et al* 2005 Self-actuated, thermo-responsive hydrogel valves for lab on a chip *Biomed. Microdevices* **7** 313–22
[25] Zeng X and Jiang H 2008 Tunable-focus microlenses actuated by infrared-light-responsive hydrogels with entrapped gold nanoparticles for fiber endoscopy *Tech. Dig. Solid-State Sensor, Actuator and Microsystems Workshop (Hilton Head Island, SC, 2008)* pp 76–79
[26] Thorslund S and Nikolajeff F 2007 Instant oxidation of closed microchannels *J. Micromech. Microeng.* **17** N16–21
[27] Haubert K, Drier T and Beebe D 2006 PDMS bonding by means of a portable, low-cost corona system *Lab Chip* **6** 1548–9
[28] Luprano V A M *et al* 1997 Non-destructive characterization of hydrogels *J. Mater. Sci. Mater. Med.* **8** 175–8
[29] Syms R R A *et al* 2003 Surface tension-powered self-assembly of micro structures—the state-of-the-art *J. Microelectromech. Syst.* **12** 387–417
[30] Rasband W S Image J US National Institutes of Health, Bethesda, MD, USA http://rsb.info.nih.gov/ij/, 1997–2009
[31] Ko H C *et al* 2008 A hemispherical electronic eye camera based on compressible silicon optoelectronics *Nature* **454** 748–53